HHS Public Access

Author manuscript

J Phys Chem B. Author manuscript; available in PMC 2022 February 18.

Published in final edited form as:

J Phys Chem B. 2021 April 08; 125(13): 3343–3352. doi:10.1021/acs.jpcb.1c00989.

Probing Side-Chain Dynamics in Proteins by NMR Relaxation of Isolated ^{13}C Magnetization Modes in $^{13}CH_3$ Methyl Groups

Vitali Tugarinov,
Laboratory of Chemical Physics, National Institute of Diabetes and Digestive and Kidney Diseases, National Institutes of Health, Bethesda, Maryland 20892-0520, United States

Alberto Ceccon,
Laboratory of Chemical Physics, National Institute of Diabetes and Digestive and Kidney Diseases, National Institutes of Health, Bethesda, Maryland 20892-0520, United States

G. Marius Clore
Laboratory of Chemical Physics, National Institute of Diabetes and Digestive and Kidney Diseases, National Institutes of Health, Bethesda, Maryland 20892-0520, United States

Abstract

The dynamics of methyl-bearing side chains in proteins were probed by ^{13}C relaxation measurements of a number of ^{13}C magnetization modes in selectively $^{13}CH_3$-labeled methyl groups of proteins. We first show how ^{13}C magnetization modes in a $^{13}CH_3$ spin-system can be isolated using acute-angle ^{1}H radio-frequency pulses. The parameters of methyl-axis dynamics, a measure of methyl-axis ordering S^2_{axis} and the correlation time of fast local methyl-axis motions (τ_f), derived from ^{13}C relaxation in $^{13}CH_3$ groups are compared with their counterparts obtained from ^{13}C relaxation in $^{13}CHD_2$ methyl isotopomers. We show that in high-molecular-weight proteins, excellent correlations are obtained between the [$^{13}CHD_2$]-derived S^2_{axis} values and those extracted from relaxation of the ^{13}C magnetization of the $I = 1/2$ manifold in $^{13}CH_3$ methyls. In smaller proteins, a certain degree of anticorrelation is observed between the S^2_{axis} and τ_f values obtained from ^{13}C relaxation of the $I = 1/2$ manifold magnetization in $^{13}CH_3$ methyls. These parameters can be partially decorrelated by inclusion in the analysis of relaxation data of the $I = 3/2$ manifold ^{13}C magnetization.

Corresponding Authors: G. Marius Clore – Laboratory of Chemical Physics, National Institute of Diabetes and Digestive and Kidney Diseases, National Institutes of Health, Bethesda, Maryland 20892-0520, United States; mariusc@mail.nih.gov, **Vitali Tugarinov** – Laboratory of Chemical Physics, National Institute of Diabetes and Digestive and Kidney Diseases, National Institutes of Health, Bethesda, Maryland 20892-0520, United States; vitali.tugarinov@nih.gov.

Supporting Information

The Supporting Information is available free of charge at https://pubs.acs.org/doi/10.1021/acs.jpcb.1c00989.
Relaxation matrices calculated in the basis set consisting of all ^{13}C magnetization modes treated in this work, comparison of the contour plots of theoretical R_2/R_1 rates of a selected set of ^{13}C magnetization modes with R_2/R_1 rates of ^{13}C nuclei in $^{13}CHD_2$ methyl groups, contributions of high frequency ($\omega > 0$) terms to the differences Δ for R_2/R_1 relaxation rates as a function of the distance to a single external ^{1}H spin, a single-transition operator-based explanation of the optimal choice of acute angle ^{1}H RF pulses, NMR sample conditions and acquisition parameters, and details of relaxation data analysis (PDF)

Complete contact information is available at: https://pubs.acs.org/10.1021/acs.jpcb.1c00989

The authors declare no competing financial interest.

Graphical Abstract

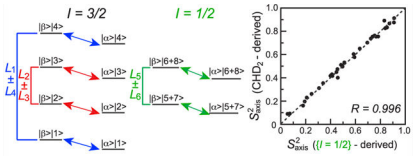

INTRODUCTION

Protein side-chain motions are one of the principal determinants of conformational entropy of protein structures[1,2] and play a significant role in molecular recognition events.[3,4] Methyl groups have long been recognized as unique probes of molecular motions and have played a special role in NMR studies of protein side-chain dynamics, providing important insights into the dynamics and thermodynamics of many biochemical processes.[5,6] The use of ^{13}C spin relaxation in $^{13}CH_3$ methyl moieties for the extraction of dynamics parameters, however, is fraught with difficulties, as the interpretation of ^{13}C relaxation in these methyl isotopomers is complicated by interference effects between dipolar fields created by the three magnetically equivalent proton spins that lead to a non-single-exponential decay of the NMR signal.[7,8] In contrast, ^{13}C relaxation in $^{13}CHD_2$ methyl isotopomers[9,10] or relaxation of ^{2}H nuclei in $^{13}CH_2D$-[11–13] or $^{13}CHD_2$-labeled[10,13,14] methyl groups present much more favorable alternatives. While relaxation of ^{2}H nuclei in $^{13}CH_2D$- and $^{13}CHD_2$-methyls, which is governed almost exclusively by quadrupolar interactions, provides the most robust probe of methyl-axis dynamics,[15] NMR experiments that quantify ^{13}C spin relaxation in $^{13}CHD_2$ methyls are generally more sensitive.[10,15] The quantitative interpretation of ^{13}C relaxation in $^{13}CHD_2$ methyl isotopomers is well established.[9,10,15] The use of $^{13}CH_3$ methyls as probes for side-chain dynamics, however, has indisputable advantages in that no special (deuterium-containing) types of isotopic labels are required and the starting sensitivity of NMR experiments targeting $^{13}CH_3$ methyls is two- to three-fold higher than those for $^{13}CH_2D$- and $^{13}CHD_2$-labeled methyl groups.[16]

Recently, we demonstrated the utility of acute (<90°)-angle ^{1}H radio frequency (RF) pulses in a variety of NMR applications that target $^{13}CH_3$ methyl groups in selectively $^{13}CH_3$-labeled and otherwise perdeuterated proteins. In particular, we showed that more efficient and sensitive selection of ^{1}H and ^{13}C transitions belonging to the $I = 1/2$ manifolds of $^{13}CH_3$ groups, which effectively reduces the complexity of a $^{13}CH_3$ spin system to the simpler case of its AX(^{13}C–^{1}H) counterpart, can be achieved with ^{1}H RF pulses adjusted to ~42°.[17] A special case of acute angle pulses, the “magic-angle” (54.7°) ^{1}H pulse, was shown to simplify and improve the sensitivity of NMR experiments that quantify the amplitudes of methyl three-fold symmetry axis motions in the case of small- to intermediate-sized proteins.[18] We further demonstrated that the transfer of magnetization to and from the slow-relaxing ^{13}C transitions of $^{13}CH_3$ methyl groups can be optimized by carefully adjusting the angles of the ^{1}H pulses in INEPT[19] transfer schemes.[20] This optimized transfer scheme was applied to methyl ^{13}C Carr–Purcell–Meiboom–Gill (CPMG)[21,22] relaxation dispersion experiments recorded on the slow-relaxing ^{13}C transitions, significantly increasing the information content of the CPMG relaxation dispersion profiles in cases where the exchange

process involved high-molecular-weight species (large protein complexes or partially aggregated states).

Here, we probe the dynamics of methyl-bearing side chains in proteins by separating groups of ^{13}C magnetization modes in $^{13}CH_3$-methyls using a variety of acute-angle ^1H RF pulses and measuring their NMR spin relaxation properties, namely transverse (R_2) and longitudinal (R_1) relaxation rates. Two parameters that describe methyl-axis dynamics—the order parameter squared of the methyl three-fold symmetry axis, S^2_{axis}, that reports on the amplitudes of methyl-axis motions and the correlation time of fast local methyl-axis motions, τ_f, that occurs on the picosecond time scale (including the rotation of the methyl group around its three-fold symmetry axis)—are extracted from relaxation rates of groups of ^{13}C magnetization modes in $^{13}CH_3$ methyls of a {U-[^2H]; Ileδ1-[$^{13}CH_3$]; Leu,Val-[$^{13}CH_3$, $^{12}CD_3$]}-labeled (ILV-{$^{13}CH_3$}) sample of the protein ubiquitin at 25 and 5 °C (MW = 8.5 kDa) and a {U-[^2H]; Ileδ1-[$^{13}CH_3$]}-labeled (Iδ1-{$^{13}CH_3$}) sample of the high-molecular-weight enzyme malate synthase G (MSG, MW = 82 kDa) at 37 °C. The $^{13}CH_3$-derived reporters of methyl-axis dynamics were compared with their counterparts derived from ^{13}C relaxation rates in $^{13}CHD_2$ methyl isotopomers using samples of the two proteins with the same labeling schemes, where the $^{13}CH_3$ methyl groups were substituted for those of the $^{13}CHD_2$ variety.

METHODS

Details regarding sample expression, purification, and isotope labeling; NMR spectroscopy; and data analysis are provided in the Supporting Information.

RESULTS AND DISCUSSION

The energy-level diagram of a $^{13}CH_3$ methyl spin system is shown in Figure 1, with the ^{13}C transitions that are the main focus of the present work shown by diagonal arrows. The diagram consists of one manifold with spin $I = 3/2$ and two manifolds with $I = 1/2$. In the macromolecular limit, transverse spin-relaxation rates of the inner ^{13}C transitions of the $I = 3/2$ manifold and those of the $I = 1/2$ manifolds are generally slower ($R^S_{2,C}$, shown with red and green arrows for the $I = 3/2$ and $I = 1/2$ manifolds, respectively; Figure 1), while the rates of the outer ^{13}C transitions of the $I = 3/2$ manifold are faster ($R^F_{2,C}$; blue arrows). By the "modes" of ^{13}C magnetization in this work, we denote classes of ^{13}C transitions (described by ^{13}C spin operators $C_+ = |\alpha\rangle\langle\beta|$ and $C_- = |\beta\rangle\langle\alpha|$), as well as the corresponding spin-order groups (populations; described by ^{13}C spin operators $C_z = (1/2)(|\alpha\rangle\langle\alpha| - |\beta\rangle\langle\beta|)$). These six ^{13}C magnetization modes are differentiated by the eight ^1H polarization states $|n\rangle\langle n|$, where the term $|n\rangle$ is a linear combination of $|i, j, k\rangle$, $i, j, k \in \{\alpha, \beta\}$ (Figure 1), and are given by

$$
\begin{aligned}
L_1 + L_4 &\equiv C_{\pm,z}(|1\rangle\langle 1| + |4\rangle\langle 4|)\\
L_2 + L_3 &\equiv C_{\pm,z}(|2\rangle\langle 2| + |3\rangle\langle 3|)\\
L_5 + L_6 &\equiv \frac{1}{\sqrt{2}} C_{\pm,z}(|5\rangle\langle 5| + |7\rangle\langle 7| + |6\rangle\langle 6| + |8\rangle\langle 8|)\\
L_1 - L_4 &\equiv C_{\pm,z}(|1\rangle\langle 1| - |4\rangle\langle 4|)\\
L_2 - L_3 &\equiv C_{\pm,z}(|2\rangle\langle 2| - |3\rangle\langle 3|)\\
L_5 - L_6 &\equiv \frac{1}{\sqrt{2}} C_{\pm,z}(|5\rangle\langle 5| + |7\rangle\langle 7| - |6\rangle\langle 6| - |8\rangle\langle 8|)
\end{aligned}
\tag{1}
$$

Relaxation decay of the modes that include raising or lowering ^{13}C spin operators ($C_{\pm}$) is described by transverse (R_2) rates, while the longitudinal rates (R_1) describe the relaxation of the modes involving longitudinal ^{13}C operators (C_z). Further, we define the subset of ^{13}C magnetization modes that involves the sums of the ^{1}H states (the first three modes in eq 1) as "in-phase" modes and those that involve the differences of ^{1}H states as "antiphase" modes.

Theoretical expressions for R_2 and R_1 spin relaxation rates of ^{13}C magnetization modes in a $^{13}CH_3$ methyl group, calculated for intra-methyl interactions using the basis set in eq 1, are presented in the Supporting Information. Here, we only include the relaxation matrix (eq 2) that describes contributions to the R_2 and R_1 rates arising from dipolar interactions with "external" proton spins (^{1}H spins outside of a given methyl moiety), as these so-called "spin-flipping" rates are central to the content of the present work.

$$
\frac{\mathrm{d}}{\mathrm{d}t}\begin{bmatrix} L_1+L_4\\ L_2+L_3\\ L_5+L_6\\ L_1-L_4\\ L_2-L_3\\ L_5-L_6 \end{bmatrix} = -k_{\mathrm{HH}}^{\mathrm{ext}} \begin{bmatrix} 1 & -1 & 0 & 0 & 0 & 0\\ -1 & 1 & 0 & 0 & 0 & 0\\ 0 & 0 & 0 & 0 & 0 & 0\\ 0 & 0 & 0 & 1 & -1 & 0\\ 0 & 0 & 0 & -1 & 11/3 & 0\\ 0 & 0 & 0 & 0 & 0 & 2/3 \end{bmatrix} \begin{bmatrix} L_1+L_4\\ L_2+L_3\\ L_5+L_6\\ L_1-L_4\\ L_2-L_3\\ L_5-L_6 \end{bmatrix}
\tag{2}
$$

where $k_{\mathrm{HH}}^{\mathrm{ext}} = \left(\frac{3}{20}\right)\left(\frac{\mu_0}{4\pi}\right)^2 \sum_{\mathrm{ext}} \frac{6\hbar^2\gamma_H^4\tau_{\mathrm{C}}}{r_{hh\mathrm{ext}}^6}$; μ_0 is the vacuum permeability constant; γ_{H} is the gyromagnetic ratio of proton spins; $r_{hh\mathrm{ext}}$ is the distance from methyl protons to an external proton spin, with the sum running over all external proton spins in the protein molecule; and τ_{C} is the global molecular rotational correlation time. Note that only the spectral density function at zero frequency, $J(0)$, is considered here, and the order parameter of the interactions with external proton spins is assumed to be unity.

Extraction of the parameters of methyl-axis dynamics from ^{13}C relaxation measurements in $^{13}CH_3$ methyl groups using ^{1}H-detected NMR experiments is hampered by (1) pervasive cross-correlations (interference) between dipolar fields created by the three magnetically equivalent ^{1}H spins (^{13}C–^{1}H/^{13}C–^{1}H and ^{1}H–^{1}H/^{1}H–^{1}H dipole–dipole cross-correlated relaxation) that lead to cross-relaxation between individual ^{13}C magnetization modes, resulting in non-single-exponential decay of coherences of interest;[7,8] and (2) dipolar

interactions of methyl protons with external ^{1}H spins. The latter contributes to (i) auto-relaxation of ^{13}C magnetization, which is difficult to quantitatively account for even when a high-resolution 3D structure of a protein is available; and (ii) cross-relaxation between ^{13}C magnetization modes that likewise results in non-single-exponential signal decay. In this work, the problem of "cross-talk" (cross-relaxation) between ^{13}C magnetization modes is alleviated by sequestering groups of ^{13}C modes of interest so that only these modes are present at the start of the relaxation delays. Meanwhile, the effects of auto-relaxation from spin-flips are mitigated by either (i) isolation of ^{13}C magnetization that is not affected by spin-flips (in-phase mode of the $I = 1/2$ manifold, $L_5 + L_6$), or (ii) corrections applied to the measured relaxation rates that are based on experimental differences between the rates of the antiphase and in-phase inner ^{13}C modes of the $I = 3/2$ manifold, $(L_2 - L_3)$ and $(L_2 + L_3)$. Note that both auto- and cross-relaxation arising from ^{1}H spin-flips are significantly reduced by high levels of deuteration of protein samples.

As in-phase ^{13}C magnetization of the $I = 1/2$ manifold ($L_5 + L_6$) is "immune" to interactions with external ^{1}H spins (the third row and column of the relaxation matrix in eq 2), we first concentrate on the isolation and measurement of the R_2 and R_1 relaxation rates of the ($L_5 + L_6$) mode using the acute-angle pulse-based methodology described earlier.[17] Figure 2 shows the pulse scheme for the measurements of $R_{1\rho}$ and R_1 relaxation rates of the ($L_5 + L_6$) ^{13}C magnetization mode. The interested reader is referred to our previous publication in ref 17 for details of ($L_5 + L_6$) sequestration from the rest of ^{13}C magnetization. Briefly, the inner slow-relaxing multiple-quantum ^{13}C–^{1}H transitions are isolated first by the initial $2\tau_b$ "purge" element of the scheme, after which a ^{1}H pulse with flip angle $\alpha = \sin^{-1}(2/3) = 41.8°$ (shown in green in Figure 2) is applied to eliminate the inner transitions of the $I = 3/2$ manifold. Subsequently, the remaining fast-relaxing ^{1}H transitions and ^{1}H triple-quantum coherences are eliminated by the second $2\tau_b$ purge element (enclosed together with the first one in the solid green box in Figure 2) and the "filtering" element with a $2\tau_c$ duration (enclosed in the dashed green box in Figure 2), respectively. Following the application of a $^{1}H_y$ pulse that polarizes only the ^{1}H transitions of the $I = 1/2$ manifold, the rest of the scheme in Figure 2 is the same as that commonly employed for ^{13}C relaxation measurements in AX(^{13}C–^{1}H) spin-systems (e.g., that of a $^{13}CHD_2$ methyl group). The measurements of R_2 and R_1 relaxation rates are thus performed on magnetization terms of the type $C_{\pm}(|5\rangle\langle 5| + |6\rangle\langle 6| + |7\rangle\langle 7| + |8\rangle\langle 8|)$ and $C_z(|5\rangle\langle 5| + |6\rangle\langle 6| + |7\rangle\langle 7| + |8\rangle\langle 8|)$, respectively (eq 1). Using the experiment shown in Figure 2, average ($L_5 + L_6$) R_2 values of 4.2 and 7.5 s^{-1} are obtained for ILV-{$^{13}CH_3$}-labeled ubiquitin at 25 and 5 °C, respectively; the corresponding ($L_5 + L_6$) R_1 values are 2.9 and 4.1 s^{-1}, respectively. Average ($L_5 + L_6$) R_2 and R_1 values of 12.1 and 0.95 s^{-1}, respectively, are obtained for ILV-{$^{13}CH_3$}-labeled MSG (37 °C).

The parameters of methyl-axis dynamics (order parameters of the methyl three-fold symmetry axis, S^2_{axis}, and correlation times of local methyl-axis motions, τ_f) derived from $^{13}CH_3$ methyl-labeled samples (see SI "Materials and Methods" for details of data analysis) are compared with their counterparts derived from ^{13}C relaxation of $^{13}CHD_2$ methyls of ubiquitin and MSG shown in Figures 3 and 4, respectively. Although good correlations are obtained for most methyl sites for the values of S^2_{axis} in ubiquitin (τ_C = 5 and 11 ns at

25 and 5 °C, respectively, in D_2O solvent), a subset of around six sites showed notably poorer agreement at both temperatures (Figure 3A and C). Better correlations are generally obtained for τ_f, with only around four methyl sites exhibiting the highest τ_f values notably overestimated in the (L_5 + L_6)-derived data set (Figures 3B and D). The disagreements between the two sets of S^2_{axis} data can be traced to the lower sensitivity of the (L_5 + L_6) R_2 rates toward S^2_{axis} compared to that of ^{13}C R_2 in the $^{13}CHD_2$ methyl groups. Figure S1 (SI) compares the contour plots or theoretical R_2 and R_1 rates of the (L_5 + L_6) mode with those of the ^{13}C nuclei in $^{13}CHD_2$ methyls as a function of [S^2_{axis}; τ_f] for τ_C = 5 ns. It can be readily appreciated from these plots that since the R_2 of (L_5 + L_6) is dependent on both S^2_{axis} and τ_f, these two parameters of dynamics can become significantly anti-correlated. As a consequence, a small error in R_1 (and hence τ_f) can result in a relatively large error of opposite sign in S^2_{axis} (the two most prominent cases of such a correlation in ubiquitin are labeled in Figure 3). Simulations show that for five of the six methyl sites with the largest disagreements in S^2_{axis} values in Figures 3A and C, a "correction" of the measured R_1 rate by only a few percent (on the order of 0.10–0.12 s^{-1} in absolute values) is sufficient to "restore" the agreement between the (L_5 + L_6)-derived and $^{13}CHD_2$-derived S^2_{axis} values. The physical origin of the lower sensitivity of the (L_5 + L_6) R_2 rates toward S^2_{axis} and the ensuing anti-correlations between S^2_{axis} and τ_f lie in the contributions to these rates from intramethyl ^1H–^1H interactions at zero frequency in the limit where the auto-relaxation spectral density is not equal to the cross-correlated relaxation one (see expressions for relaxation rates in SI), which is notably absent from ^{13}C R_2 rates in $^{13}CHD_2$ isotopomers.

In larger protein molecules such as MSG, with τ_C = 46 ns (assumed isotropic) at 37 °C in D_2O, the (L_5 + L_6) R_2 and R_1 rates are separated in their information content in the sense that R_2 reports almost exclusively on S^2_{axis}, while R_1 is dependent exclusively on τ_f. This is a direct consequence of the (near) equality of the auto- and cross-correlated relaxation spectral density functions in the limit where $\tau_C \gg \tau_f$. Therefore, the sensitivity of the (L_5 + L_6) R_2 rates with respect to S^2_{axis} is "restored" in this case, and the agreement between the (L_5 + L_6)-derived S^2_{axis} values and their $^{13}CHD_2$-derived counterparts is excellent for almost all Ileδ1 methyl sites in MSG (Figure 4A; see SI "Materials and Methods" for experimental details of the relaxation measurements). The contour plots of theoretical (L_5 + L_6) relaxation rates are compared with the ^{13}C rates in $^{13}CHD_2$ isotopomers as a function of [S^2_{axis}; τ_f] for τ_C = 60 ns in Figure S2 (SI). As the τ_C value of MSG is strongly dependent on the protein concentration in the NMR sample (ranging from ~46 ns for a 0.5 mM sample to ~64 ns for a 1.1 mM sample), we have chosen, for the purposes of illustration, to make the plots for a τ_C value closer to the upper limit of this range.

The correlations obtained between the two sets of τ_f data for MSG (Figure 4B) are notably inferior to those for smaller proteins (cf. Figure 4B and Figure 3B and D). This is not surprising considering the large contributions of ^1H–^1H dipolar interactions to the (L_5 + L_6) R_1 rates, whereas ^{13}C R_1 rates in $^{13}CHD_2$ methyls are not affected by these interactions.

The worst agreement between the two sets of τ_f data is noted for methyl sites with the lowest S^2_{axis} values (where the part of the spectral density that accounts for local motions is the largest). Therefore, six such methyl sites were eliminated from the plot in Figure 4B. We note that the systematic underestimation of τ_f values derived from the (L_5 + L_6) rates compared to their $^{13}CHD_2$-derived counterparts (apparent in Figure 4B) is unlikely to arise from differences in dynamics between $^{13}CH_3$ and $^{13}CHD_2$ methyl isotopomers (as the same trend is not observed for ubiquitin in Figures 3B and D) and is probably an artifact of the modeling of the spectral density function (see SI for details).

In an attempt to improve the agreement between the (L_5 + L_6)-derived and $^{13}CHD_2$-derived measures of methyl-axis dynamics for small- to medium-sized proteins, we explored the possibility of using the relaxation properties of other ^{13}C magnetization modes in a $^{13}CH_3$ spin system. The fast-relaxing (outer) ^{13}C transitions (shown in blue in Figure 1) and the corresponding spin orders ($L_1 \pm L_4$) present a potentially attractive choice because of (1) the steep dependence of ($L_1 \pm L_4$) R_2 rates on S^2_{axis} (see Figure S1; the lower row of panels shows the contour plots of (L_1 + L_4) R_2/R_1 as a function of [S^2_{axis};τ_f]) and (2) the absence of contributions from intramethyl ^1H–^1H interactions at zero frequency to ($L_1 \pm L_4$) R_2/R_1 rates (see expressions for the relaxation rates in the SI). Note that both R_2 and R_1 rates of the antiphase magnetization ($L_1 - L_4$) are predicted to be very similar to those of the in-phase (L_1 + L_4) magnetization for deuterated proteins (down to very short distances to external ^1H spins, ~2.5 Å). However, both auto- and cross-relaxation rates of the ($L_1 \pm L_4$) mode have contributions from spin flips (eq 2). Although the contributions to R_2 from spin flips are not predicted to exceed a few percent of the total rate in deuterated protein samples (a maximal value of ~6% is calculated for the shortest effective distance to an external ^1H spin in deuterated ILV-{$^{13}CH_3$}-ubiquitin), the R_1 rates are affected more significantly—up to ~40% of the total rate for ubiquitin at 5 °C. In larger proteins the size of MSG, spin flips are predicted to dominate the ($L_1 \pm L_4$) R_1 rates (>50% of the total), making them practically uninterpretable. Nevertheless, as long as the rate of spin flips does not dominate the longitudinal relaxation decay, and individual ^{13}C magnetization modes are isolated prior to the relaxation delay, minimizing the effect of cross-relaxation between different modes, these contributions can be approximately corrected for. Indeed, close inspection of the expressions for relaxation rates of all magnetization modes (see SI) shows that the difference between the rates of decay (R_2 or R_1) of the antiphase and in-phase inner magnetization modes of the I = 3/2 manifold, ($L_2 - L_3$) and (L_2 + L_3), respectively, represents the most accurate measure of spin-flipping rates in the macromolecular limit (see eqs S5.1 and S5.2 and Figure S3 in the SI). According to eq 2, this difference is $\Delta = R_{(L2-L3)} - R_{(L2+L3)} \approx (8/3)k^{ext}_{HH}$. Once estimated experimentally from the $R_{(L2-L3)}$ and $R_{(L2+L3)}$ rates, the value of Δ can then be scaled by a factor of 3/8 to be used as a correction for spin flips for R_2/R_1 rates of the ($L_1 \pm L_4$) mode. Note that rather than relying on an estimation of distances to external protons from the protein structure, such a correction is entirely based on the relaxation properties of a $^{13}CH_3$ spin system.

The pulse schemes designed for the isolation and relaxation measurements of the ($L_1 \pm L_4$) and ($L_2 \pm L_3$) ^{13}C magnetization modes in $^{13}CH_3$ methyls are shown in Figures 5 and 6,

respectively, and rely on the use of acute-angle ^{1}H pulses. Both schemes start with selection of fast-relaxing multiple-quantum ^{13}C–^{1}H magnetization using purge elements of duration $4\tau_b$ (enclosed in solid blue and red boxes in Figures 5 and 6, respectively). In the scheme for $(L_1 \pm L_4)$ selection in Figure 5, this element is followed by a $^{1}H_y$ pulse applied with a flip angle β equal to the "magic" angle $\cos^{-1}(1/\sqrt{3}) = 54.7°$ (shown in blue), which selectively polarizes the outer ^{1}H magnetization states ($|1\rangle\langle 1|$ and $|4\rangle\langle 4|$, Figure 1; see SI for details) so that magnetization terms of the type $C_{\pm}(|1\rangle\langle 1| \pm |4\rangle\langle 4|)$ and $C_z(|1\rangle\langle 1| \pm |4\rangle\langle 4|)$ can be generated for R_2 and R_1 measurements, respectively. In the experiment for the selection of $(L_2 \pm L_3)$ in Figure 6, the selection of fast-relaxing multiple-quantum ^{13}C–^{1}H magnetization is followed by a $^{1}H_y$ 90° pulse to polarize all the ^{1}H states of the $I = 3/2$ manifold($|1\rangle\langle 1|$, $|2\rangle\langle 2|$, $|3\rangle\langle 3|$ and $|4\rangle\langle 4|$; Figure 1), which is followed by selection of the desired ^{1}H states ($|2\rangle\langle 2|$, $|3\rangle\langle 3|$) by a "filtering" element of $2\tau_c$ duration (enclosed in a dashed red box in Figure 6) and subsequent generation of the magnetization terms $C_{\pm}(|2\rangle\langle 2| \pm |3\rangle\langle 3|)$ and $C_z(|2\rangle\langle 2| \pm |3\rangle\langle 3|)$ for R_2 and R_1 measurements, respectively. Note that to maximize the transfer of magnetization from ^{13}C coherences of the type $C_{\pm,z}(|2\rangle\langle 2| - |3\rangle\langle 3|)$ to the slow-relaxing component of the multiple-quantum ^{13}C–^{1}H magnetization $C_{\pm}(|2\rangle\langle 3| + |3\rangle\langle 2|)$, a ^{1}H pulse with flip angle $\gamma = \sin^{-1}(\sqrt{8}/27) = 33°$ is applied (shown in red in Figure 6; see the SI for details), followed by a purge element $2\tau_b$ that selects for the slow-relaxing part of the (multiple-quantum) magnetization before the t_1 evolution period.

It is worth emphasizing that relaxation measurements of the $(L_1 \pm L_4)$ and $(L_2 \pm L_3)$ magnetization modes (Figures 5 and 6, respectively) are more technically demanding by far than those of the $(L_5 \pm L_6)$ magnetization mode in Figure 2. One of the underlying difficulties arises from cross-relaxation between the $(L_1 \pm L_4)$ and $(L_2 \pm L_3)$ modes, which is induced by spin-flips (eq 2) that make the relaxation decay of these terms non-single-exponential for at least some methyl sites. Although perdeuteration of NMR samples mitigates this effect, it cannot be eliminated completely. Therefore, care should be exercised not to extend relaxation delays to excessively large values. Further, in the measurement of $(L_1 \pm L_4)$ R_2 rates (Figure 5), we have chosen not to apply a spin-lock RF field to (1) avoid problems associated with large values of the ^{1}H–^{13}C scalar couplings operative for the outer (fast-relaxing) ^{13}C transitions ($3^{1}J_{CH} \sim 380$ Hz; the 2 kHz spin-lock field, typically employed in other experiments, may be only marginally sufficient for couplings of this magnitude; note that the "free-precession" R_2 values should not be affected by the differences between in-phase $(L_1 + L_4)$ and antiphase $(L_1 - L_4)$ R_2 rates as these are predicted to be very small in deuterated proteins); and (2) mitigate the effect of spin flips, which are expected to be reduced as the cross-relaxing components of the magnetization are secular in the absence of the RF field. In addition, ^{1}H 180° pulses applied during relaxation delays to eliminate methyl ^{13}C CSA and ^{13}C–^{1}H dipolar cross correlations in the measurements involving antiphase magnetization, i.e., $(L_1 - L_4)$ or $(L_2 - L_3)$, have to be implemented as composite pulses with the phase cycling as described in Figures 5 and 6. Using the pulse scheme in Figure 5, average $(L_1 \pm L_4)$ R_2 rates of 12.5 and 24.3 s^{-1} were obtained for ILV-{$^{13}CH_3$}-labeled ubiquitin at 25 and 5 °C, respectively, while the corresponding average R_1 rates were 3.8 and 4.2 s^{-1}, respectively. The average $(L_2 + L_3)$ R_2 and R_1 rates were 4.3 and 3.3 s^{-1}, respectively, at 25 °C, and 7.0 and 6.0 s^{-1} at 5 °C, while their antiphase counterparts $(L_2 - L_3)$ had average values of 6.4 and 5.4 s^{-1},

respectively, at 25 °C and 11.4 and 10.3 s^{-1}, respectively, at 5 °C. The ($L_1 \pm L_4$) R_2 and R_1 rates of all methyl sites were corrected (on a site-specific basis) by the experimental value of $k_{HH}^{ext} = (3/8)\Delta$, where Δ is the difference between the R_2/R_1 rates of the antiphase ($L_2 - L_3$) and in-phase ($L_2 + L_3$) modes as described above. The average corrections employed for the R_2 and R_1 rates were 0.79 and 0.78 s^{-1}, respectively, at 25 °C, and 1.64 and 1.62 s^{-1}, respectively, at 5 °C.

By themselves, the thus-corrected relaxation rates of the ($L_1 \pm L_4$) modes are not (on average) as good measures of methyl-axis dynamics as those of the ($L_5 + L_6$) ^{13}C magnetization. Although it may be tempting to include the (corrected) ($L_1 \pm L_4$) relaxation rates in the analysis only for those methyl sites that show the worst agreement between the two sets of dynamics parameters in Figure 3, we prefer to do so for *all* ILV methyl groups of ubiquitin since in the absence of the "benchmark" set of $^{13}CHD_2$-derived parameters [S^2_{axis}; τ_f] it would not be possible to know *a-priori* which methyl sites are compromised (where S^2_{axis} is anticorrelated with τ_f). Note that the ($L_2 + L_3$) rates are not included in the analysis directly as, in the absence of spin flips, the ($L_2 + L_3$) relaxation rates are very similar (to within experimental errors) to those of the ($L_5 + L_6$) mode and, therefore, are not expected to provide additional information on methyl-axis dynamics.

Figure 7 shows correlation plots comparing methyl-axis dynamics parameters derived from ^{13}C relaxation of the ($L_5 + L_6$) mode ($I = 1/2$ manifold) complemented with the R_2/R_1 rates of ($L_1 \pm L_4$) in $^{13}CH_3$ methyl groups with those derived from ^{13}C relaxation in $^{13}CHD_2$ isotopomers of ubiquitin. A notable improvement is observed in the quality of the correlations for S^2_{axis} at both temperatures (Figures 7A and C) compared to the plots where only the ($L_5 + L_6$) data are used (cf. Figures 3A and C). The agreement in τ_f is likewise ameliorated for the four methyl sites with the highest τ_f values (Figures 7B and D). Note that inclusion of the ($L_1 \pm L_4$) R_2/R_1 data in the analysis (see SI "Materials and Methods"), increases the number of degrees of freedom in the fit from zero to two, providing additional information content that at least partially overcomes correlations between S^2_{axis} and τ_f.

In the absence of relaxation, experiments for the measurement of $R_{1\rho}$ and R_1 relaxation rates of the ($L_5 + L_6$) magnetization mode (Figure 2) are predicted to be around threefold less sensitive than the experiments designed for relaxation measurements in $^{13}CHD_2$ methyl isotopomers.[17] As discussed previously, transverse relaxation during the $4\tau_b$ and $2\tau_a$ periods in the pulse scheme of Figure 2, and slower longitudinal ^1H relaxation in $^{13}CHD_2$ methyls during recovery delays, can increase or reduce this factor, respectively.[17] These predictions are borne out in this work, with sensitivity ratios for the two types of experiments of 0.42 and 0.38 measured for ubiquitin and MSG, respectively, for the first point of the relaxation series ($T = 0$) when using a recovery delay of 1.5 s. In the absence of relaxation, the sensitivity of the experiments selecting for the ($L_1 \pm L_4$) and ($L_2 \pm L_3$) magnetization modes in Figures 5 and 6, respectively, is related to that selecting for the ($L_5 + L_6$) mode in Figure 2 in a ratio of 2.68:1.04:1.0, where the sensitivity enhancement of the experiment in Figure 2 by √2 is taken into account. However, as both experiments that target the $I = 3/2$ manifold modes (Figures 5 and 6) start with the selection of the fast-relaxing methyl

coherences and, in the case of the experiment in Figure 5, the fast-relaxing ^{1}H coherences are included during signal detection (the acquisition period), these experiments are less tolerant to transverse relaxation. While the measured ratio of sensitivities is 1.95:0.88:1.0 for ubiquitin at 5 °C, we predict that the sensitivity of both experiments in Figures 5 and 6 will be significantly lower for much larger proteins than that of the experiment in Figure 2.

Numerical simulations of sensitivity of the relaxation rates obtained in the experiments described here to mis-settings of the ^{1}H acute-angle pulses show that $R_2(R_{1\rho})$ relaxation rates measured in the experiment in Figure 2 (the selection of the (L_5 + L_6) magnetization modes) are quite sensitive to inaccuracies of the pulse with flip angle α. The relative sensitivity of the extracted R_2 rates is predicted to be inversely proportional to the global molecular correlation time τ_C; changes of ~1.5% in the R_2 rate per one degree of α-angle mis-setting are obtained for MSG (τ_C ~ 46 ns), and values of ~2.5% and ~2.8% per degree are obtained for ubiquitin at 25 and 5 °C, respectively (τ_C ~ 5 and 11 ns, respectively). R_1 rates obtained in the same experiment (Figure 2) are relatively less sensitive to the mis-calibration of the α-pulse, with values of less than ~0.5% per degree predicted for the whole range of τ_C values studied here. It is worth noting that the ^{1}H 90° “purging” pulse applied to “in-phase” magnetization (L_5 + L_6) immediately before the relaxation delay (the inset in Figure 2) substantially mitigates these effects. In contrast, both R_2 and R_1 relaxation rates of the ($L_1 \pm L_4$) magnetization modes (pulse scheme in Figure 5) are quite insensitive to the mis-setting of the β-angle, with relative sensitivities of only ~0.2% and ~0.1% per degree obtained for R_2 and R_1 rates in ubiquitin (5 °C), respectively. Note that relaxation rates of the ($L_2 \pm L_3$) magnetization modes (pulse scheme in Figure 6) should not depend on the mis-setting of angle γ, as this angle is not used for the selection proper of the ($L_2 \pm L_3$) modes and is optimized solely to improve the sensitivity of the experiment.

CONCLUSIONS

In summary, we have described the dynamics of methyl-bearing side-chains in proteins by ^{13}C relaxation measurement of a number of modes (classes) of ^{13}C magnetization in selectively $^{13}CH_3$-labeled methyl groups of otherwise deuterated proteins. We first show how the ^{13}C magnetization modes whose NMR relaxation properties, transverse (R_2) and longitudinal (R_1) spin relaxation rates, bear information on the methyl-axis dynamics in $^{13}CH_3$ methyl groups, can be isolated using acute-angle ^{1}H RF pulses. The parameters of methyl-axis dynamics (S^2_{axis}, a measure of the amplitudes of the methyl-axis motions, and τ_f, the correlation time of the fast local methyl-axis motions) derived from ^{13}C relaxation in $^{13}CH_3$ methyls are compared with their counterparts derived from ^{13}C relaxation in $^{13}CHD_2$ methyl isotopomers. We show that excellent correlations between the [$^{13}CHD_2$]-derived S^2_{axis} values and those extracted from relaxation of ^{13}C magnetization of the I = 1/2 manifold in $^{13}CH_3$ methyls can be obtained in larger proteins. In $^{13}CH_3$ methyls of smaller proteins, a certain degree of anti-correlation is observed between S^2_{axis} and τ_f values obtained from ^{13}C relaxation of the I = 1/2 manifold magnetization. This correlation can be (partially) removed by inclusion in the analysis of ^{13}C relaxation data acquired on the I = 3/2 manifold magnetization modes.

Supplementary Material

Refer to Web version on PubMed Central for supplementary material.

ACKNOWLEDGMENTS

We are grateful to Prof. Lewis E. Kay for many useful discussions and productive suggestions. We also thank Drs. James Baber, Jinfa Ying, and Dan Garrett for technical support. This work was supported by the Intramural Program of the National Institute of Diabetes and Digestive and Kidney Diseases, National Institutes of Health (DK029023 to G.M.C.).

REFERENCES

(1). Akke M; Brüschweiler R; Palmer AG NMR Order Parameters and Free Energy: An Analytic Approach and Application to Cooperative Calcium Binding by Calbindin D9k. J. Am. Chem. Soc 1993, 115, 9832–9833.

(2). Igumenova TI; Frederick KK; Wand AJ Characterization of the Fast Dynamics of Protein Amino Acid Side Chains Using NMR Relaxation in Solution. Chem. Rev 2006, 106, 1672–1699. [PubMed: 16683749]

(3). Frederick KK; Marlow MS; Valentine KG; Wand AJ Conformational Entropy in Molecular Recognition by Proteins. Nature 2007, 448, 325–329. [PubMed: 17637663]

(4). Sprangers R; Kay LE Quantitative Dynamics and Binding Studies of the 20s Proteasome by NMR. Nature 2007, 445, 618–622. [PubMed: 17237764]

(5). Rosenzweig R; Kay LE Bringing Dynamic Molecular Machines into Focus by Methyl-Trosy NMR. Annu. Rev. Biochem 2014, 83, 291–315. [PubMed: 24905784]

(6). Schütz S; Sprangers R Methyl Trosy Spectroscopy: A Versatile NMR Approach to Study Challenging Biological Systems. Prog. Nucl. Magn. Reson. Spectrosc 2020, 116, 56–84. [PubMed: 32130959]

(7). Kay LE; Bull TE; Nicholson LK; Griesinger C; Schwalbe H; Bax A; Torchia DA The Measurement of Heteronuclear Transverse Relaxation Times in AX3 Spin Systems Via Polarization Transfer Techniques. J. Magn. Reson 1992, 100 (3), 538–558.

(8). Kay LE; Torchia DA The Effects of Dipolar Cross-Correlation on 13C Methyl-Carbon T1, T2, and NOE Measurements in Macromolecules. J. Magn. Reson 1991, 95 (3), 536–547.

(9). Ishima R; Petkova AP; Louis JM; Torchia DA Comparison of Methyl Rotation Axis Order Parameters Derived from Model-Free Analyses of ^{2}H and ^{13}C Longitudinal and Transverse Relaxation Rates Measured in the Same Sample. J. Am. Chem. Soc 2001, 123, 6164–6171. [PubMed: 11414851]

(10). Tugarinov V; Kay LE Quantitative ^{13}C and ^{2}H NMR Relaxation Studies of the 723-Residue Enzyme Malate Synthase G Reveal a Dynamic Binding Interface. Biochemistry 2005, 44, 15970–15977. [PubMed: 16331956]

(11). Muhandiram DR; Yamazaki T; Sykes BD; Kay LE Measurement of Deuterium T_1 and $T_{1\rho}$ Relaxation Times in Uniformly ^{13}C Labeled and Fractionally Deuterium Labeled Proteins in Solution. J. Am. Chem. Soc 1995, 117, 11536–11544.

(12). Millet O; Muhandiram DR; Skrynnikov NR; Kay LE Deuterium Spin Probes of Side-Chain Dynamics in Proteins. 1. Measurement of Five Relaxation Rates Per Deuteron in ^{13}C-Labeled and Fractionally ^{2}H-Enriched Proteins in Solution. J. Am. Chem. Soc 2002, 124, 6439–6448. [PubMed: 12033875]

(13). Tugarinov V; Ollerenshaw JE; Kay LE Probing Side-Chain Dynamics in High Molecular Weight Proteins by Deuterium NMR Spin Relaxation: An Application to an 82-kDa Enzyme. J. Am. Chem. Soc 2005, 127, 8214–8225. [PubMed: 15926851]

(14). Tugarinov V; Kay LEA 2H NMR Relaxation Experiment for the Measurement of the Time Scale of Methyl Side-Chain Dynamics in Large Proteins. J. Am. Chem. Soc 2006, 128, 12484–12489. [PubMed: 16984199]

(15). Sheppard D; Sprangers R; Tugarinov V Experimental Approaches for NMR Studies of Side-Chain Dynamics in High-Molecular-Weight Proteins. Prog. Nucl. Magn. Reson. Spectrosc 2010, 56, 1–45. [PubMed: 20633347]

(16). Ollerenshaw JE; Tugarinov V; Skrynnikov NR; Kay LE Comparison of $^{13}CH_3$, $^{13}CH_2D$, and $^{13}CHD_2$ Methyl Labeling Strategies in Proteins. J. Biomol. NMR 2005, 33, 25–41. [PubMed: 16222555]

(17). Tugarinov V; Karamanos TK; Ceccon A; Clore GM Optimized NMR Experiments for the Isolation of I = 1/2 Manifold Transitions in Methyl Groups of Proteins. ChemPhysChem 2020, 21, 13–19. [PubMed: 31703148]

(18). Tugarinov V; Karamanos TK; Clore GM Magic-Angle-Pulse Driven Separation of Degenerate ^1H Transitions in Methyl Groups of Proteins: Application to Studies of Methyl Axis Dynamics. ChemPhysChem 2020, 21, 1087–1091. [PubMed: 32246547]

(19). Morris GA; Freeman R Enhancement of Nuclear Magnetic Resonance Signals by Polarization Transfer. J. Am. Chem. Soc 1979, 101, 760–762.

(20). Tugarinov V; Karamanos TK; Clore GM Optimized Selection of Slow-Relaxing 13C Transitions in Methyl Groups of Proteins: Application to Relaxation Dispersion. J. Biomol. NMR 2020, 74, 673–680. [PubMed: 33006092]

(21). Carr HY; Purcell EM Effects of Diffusion on Free Precession in Nuclear Magnetic Resonance Experiments. Phys. Rev 1954, 94, 630–638.

(22). Meiboom S; Gill D Modified Spin-Echo Method for Measuring Nuclear Relaxation Times. Rev. Sci. Instrum 1958, 29, 688–691.

(23). Shaka AJ; Keeler J; Frenkiel T; Freeman R An Improved Sequence for Broadband Decoupling: Waltz-16. J. Magn. Reson 1983, 52 (2), 335–338.

(24). Griesinger C; Ernst RR Frequency Offset Effects and Their Elimination in NMR Rotating-Frame Cross-Relaxation Spectroscopy. J. Magn. Reson 1987, 75 (2), 261–271.

(25). Yamazaki T; Muhandiram R; Kay LE NMR Experiments for the Measurement of Carbon Relaxation Properties in Highly Enriched, Uniformly ^{13}C, ^{15}N Labeled Proteins: Application to $^{13}C^{\alpha}$ Carbons. J. Am. Chem. Soc 1994, 116, 8266–8278.

(26). Kay LE; Keifer P; Saarinen T Pure Absorption Gradient Enhanced Heteronuclear Single Quantum Correlation Spectroscopy with Improved Sensitivity. J. Am. Chem. Soc 1992, 114, 10663–10665.

(27). Schleucher J; Sattler M; Griesinger C Coherence Selection by Gradients without Signal Attenuation: Application to the Three-Dimensional HNCO Experiment. Angew. Chem. Int. Ed. Engl 1993, 32, 1489–1491.

(28). Marion D; Ikura M; Tschudin R; Bax A Rapid Recording of 2D NMR Spectra without Phase Cycling. Application to the Study of Hydrogen Exchange in Proteins. J. Magn. Reson 1989, 85, 393–399.

(29). Levitt MH Symmetrical Composite Pulse Sequences for NMR Population Inversion. II. Compensation of Resonance Offset. J. Magn. Reson 1982, 50, 95–110.

(30). Gullion T; Baker DB; Conradi MS New, Compensated Carr-Purcell Sequences. J. Magn. Reson 1990, 89, 479–484.

(31). Yuwen T; Huang R; Vallurupalli P; Kay LE A Methyl-Trosy-Based ^1H Relaxation Dispersion Experiment for Studies of Conformational Exchange in High Molecular Weight Proteins. Angew. Chem. Int. Ed 2019, 58, 6250–6254.

(32). States DJ; Haberkorn RA; Ruben DJ A Two-Dimensional Nuclear Overhauser Experiment with Pure Absorption Phase in Four Quadrants. J. Magn. Reson 1982, 48 (2), 286–292.

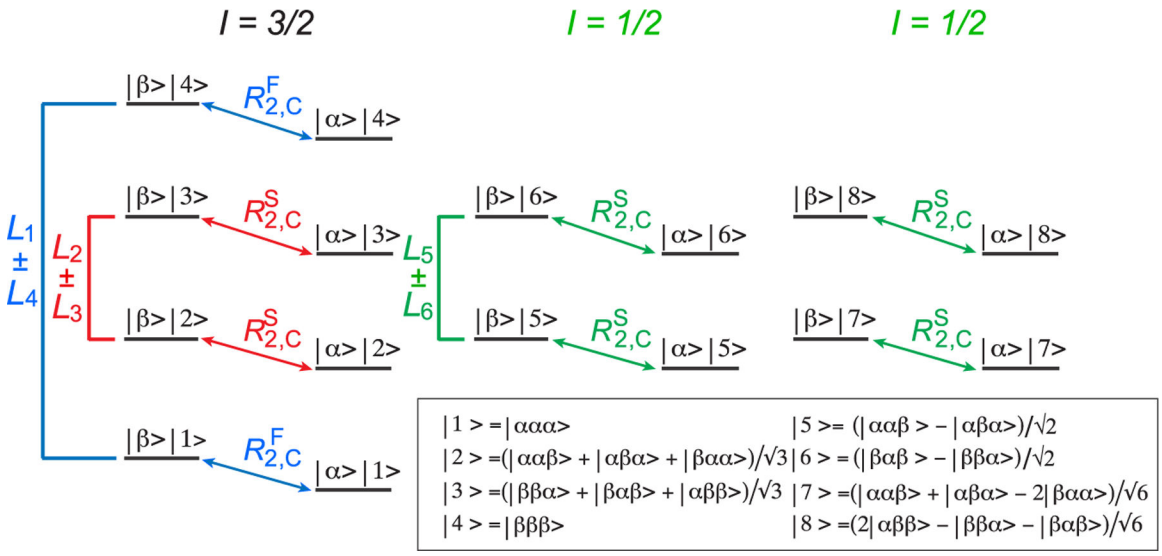

Figure 1.

Energy level diagram of the $^{13}CH_3$ (AX_3) spin-system of a methyl group. Single-quantum ^{13}C transitions are shown by diagonal arrows. The slow- and fast-relaxing ^{13}C ($R_{2,C}$) transitions are distinguished by the superscripts “S” and “F”, respectively. The spin quantum numbers, I, of the three manifolds are specified below the energy-level diagram. The slow- and fast-relaxing ^{13}C transitions of the $I = 3/2$ manifold are colored in red and blue, respectively, while the transitions of the $I = 1/2$ manifold are colored in green. Various ^{13}C magnetization modes isolated in the NMR experiments are denoted by $L_i \pm L_j$ ($i,j \in \{1–6\}$) and shown using the same coloring scheme. All 16 eigenstates are denoted by $|m\rangle|n\rangle$, where $|m\rangle$ is the state of the ^{13}C spin, $m \in \{\alpha, \beta\}$, and the eight ^1H eigenstates $|n\rangle$ are described by linear combinations of $|i, j, k\rangle$ ($i, j, k \in \{\alpha, \beta\}$) as shown below the diagram.

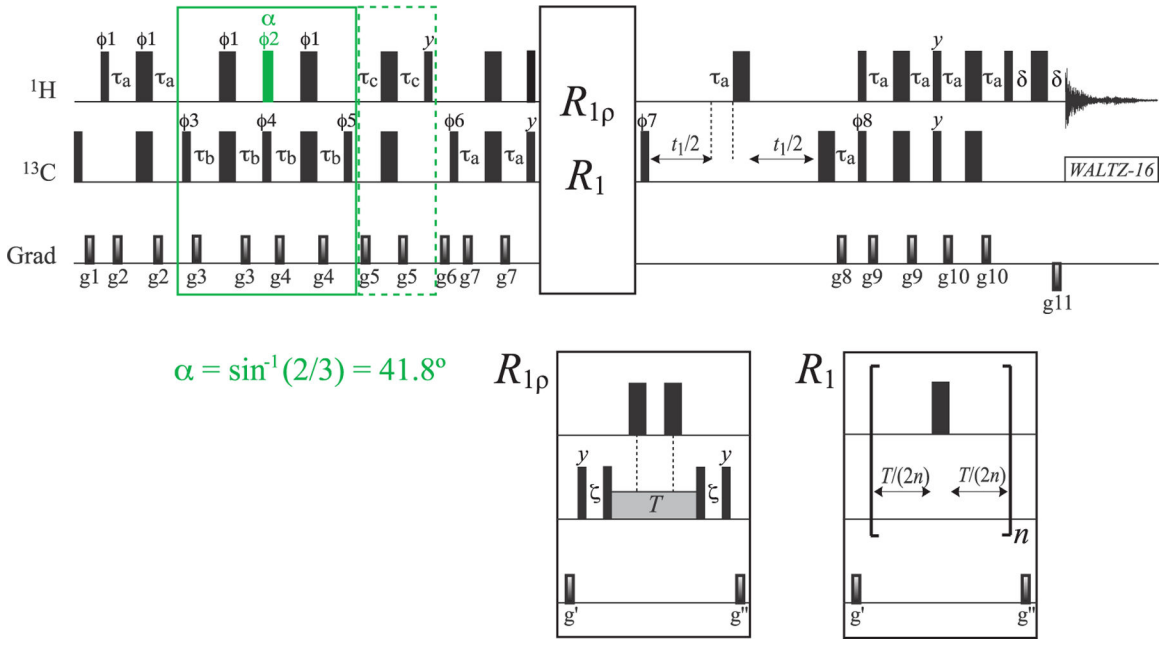

Figure 2.

Pulse scheme for the measurement of $R_{1\rho}$ and R_1 relaxation rates of the ^{13}C magnetization mode ($L_5 + L_6$) ($I = 1/2$ manifold) in $^{13}CH_3$ methyl groups. All narrow and wide rectangular pulses are applied with flip angles of 90° and 180°, respectively, along the x-axis unless indicated otherwise. For ILV-{$^{13}CH_3$}-labeled samples, the ^1H and ^{13}C carrier frequencies are positioned at 0.5 and 20 ppm, respectively, in the center of the Ileδ1-Leu-Val methyl region; for Iδ1-{$^{13}CH_3$}-labeled samples, the ^1H and ^{13}C carrier frequencies are set to 0.7 and 12 ppm, respectively. All ^1H and ^{13}C pulses are applied with the highest possible power, while ^{13}C WALTZ-16 decoupling[23] is achieved using a 2 kHz field. The ^1H pulse colored in green is applied with flip angle α equal to $\sin^{-1}(2/3) = 41.8°$. Delays are $\tau_a = 1/(4J_{HC}) = 2.0$ ms; $\tau_b = 1/(8J_{HC}) = 1.0$ ms; $\tau_c = 1/(12J_{HC}) = 0.67$ ms; $\delta = 300$ μs; and $\zeta = 1/(2\pi \times B_{SL}) - (4/\pi) \times$ pwc,[24,25] where B_{SL} is the strength of ^{13}C spin-lock field (Hz) applied along the x-axis, "pwc" is the length of the ^{13}C 90° (high power) pulse. T is a variable relaxation delay. The durations and strengths of the pulsed-field gradients (ms; G/cm) are as follows: g1 = (1; 25), g2 = (0.4; 15), g3 = (0.3; 12), g4 = (0.35; 15), g5 = (0.2; 20), g6 = (1.2; −15), g7 = (0.4; 12), g8 = (0.2; 35), g9 = (0.5; 12), g10 = (0.4; 12), g11= (0.053; −35), g′ = (1.2; 12), and g″ = (0.8; 10). The phase cycle is as follows: $\phi1 = x$; $\phi2 = 2(y), 2(-y)$; $\phi3 = 2(x), 2(-x)$; $\phi4 = y, -y$; $\phi5 = 4(x), 4(-x)$; $\phi6 = 2(x), 2(-x)$; $\phi7 = x, -x$; $\phi8 = x$; receiver phase $= 2(x, -x), 2(-x, x)$. Quadrature detection in t_1 is achieved in a Rance-Kay mode[26,27] by recording a pair of data sets for each value of t_1 corresponding to ($\phi8$, g8) and ($-\phi8$, −g8). The phase $\phi7$ is incremented by 180° along with the phase of the receiver for each complex t_1 point.[28]

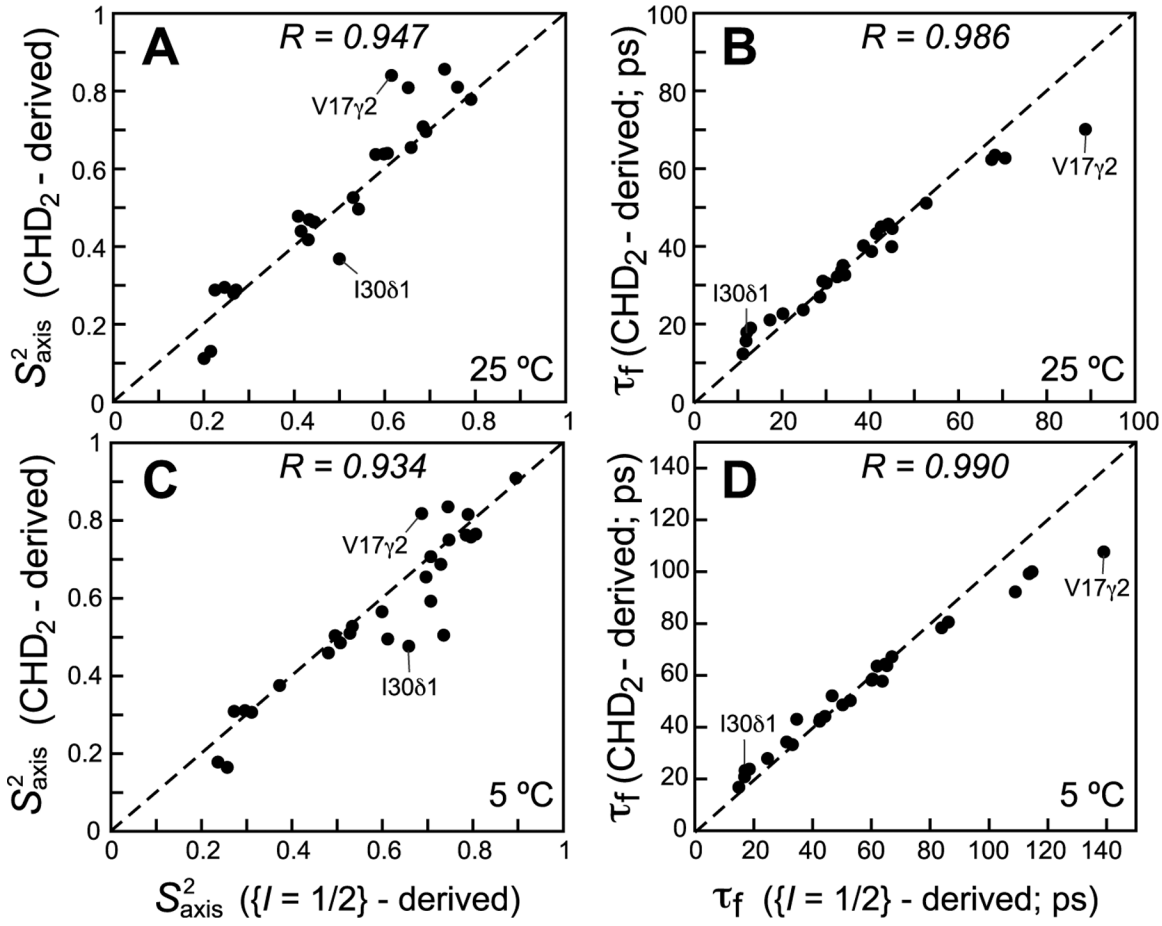

Figure 3.

Correlation plots comparing methyl-axis dynamics parameters derived from ^{13}C relaxation measurements of the ($L_5 + L_6$) magnetization mode ($I = 1/2$ manifold) in $^{13}CH_3$ methyls using the scheme in Figure 2 (*x*-axes) with those derived from ^{13}C relaxation in $^{13}CHD_2$ methyls (*y*-axes) for ILV-labeled samples of ubiquitin at 25 °C (upper row; (**A**) S^2_{axis} and (**B**) τ_f; 29 correlations) and 5 °C (lower row; (**C**) S^2_{axis} and (**D**) τ_f; 30 correlations). All data were collected at 600 MHz. The data for the L50δ2 and L56δ2 methyl sites were excluded from the plots because of large exchange contributions to their R_2 values. Linear correlation coefficients are shown at the top of each plot. Dashed lines are drawn at $y = x$.

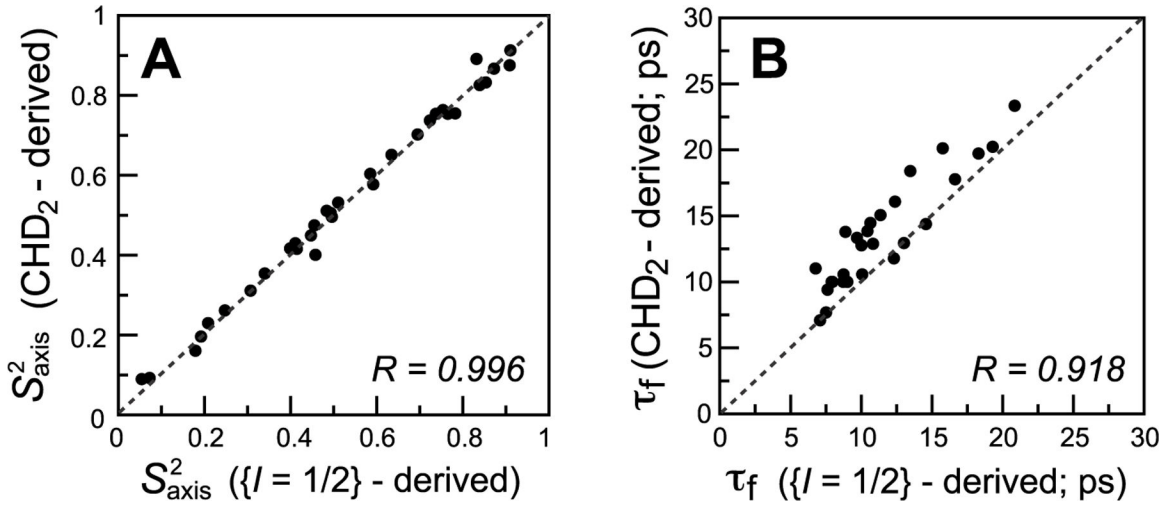

Figure 4.

Correlation plots comparing methyl-axis dynamics parameters derived from ^{13}C relaxation measurements of the (L_5 + L_6) magnetization mode (I = 1/2 manifold) in $^{13}CH_3$ methyls using the scheme in Figure 2 (x-axes) with those derived from ^{13}C relaxation in $^{13}CHD_2$ methyls (y-axes) for Ileδ1-labeled samples of MSG at 37 °C (600 MHz). (**A**) S^2_{axis} and (**B**) τ_f (ps). Linear correlation coefficients are shown at the lower right corner of each plot. Dashed lines are drawn at $y = x$. A total of 33 correlations are included in panel A, and 27 correlations in panel B with 6 correlations showing the lowest S^2_{axis} values excluded from the plot.

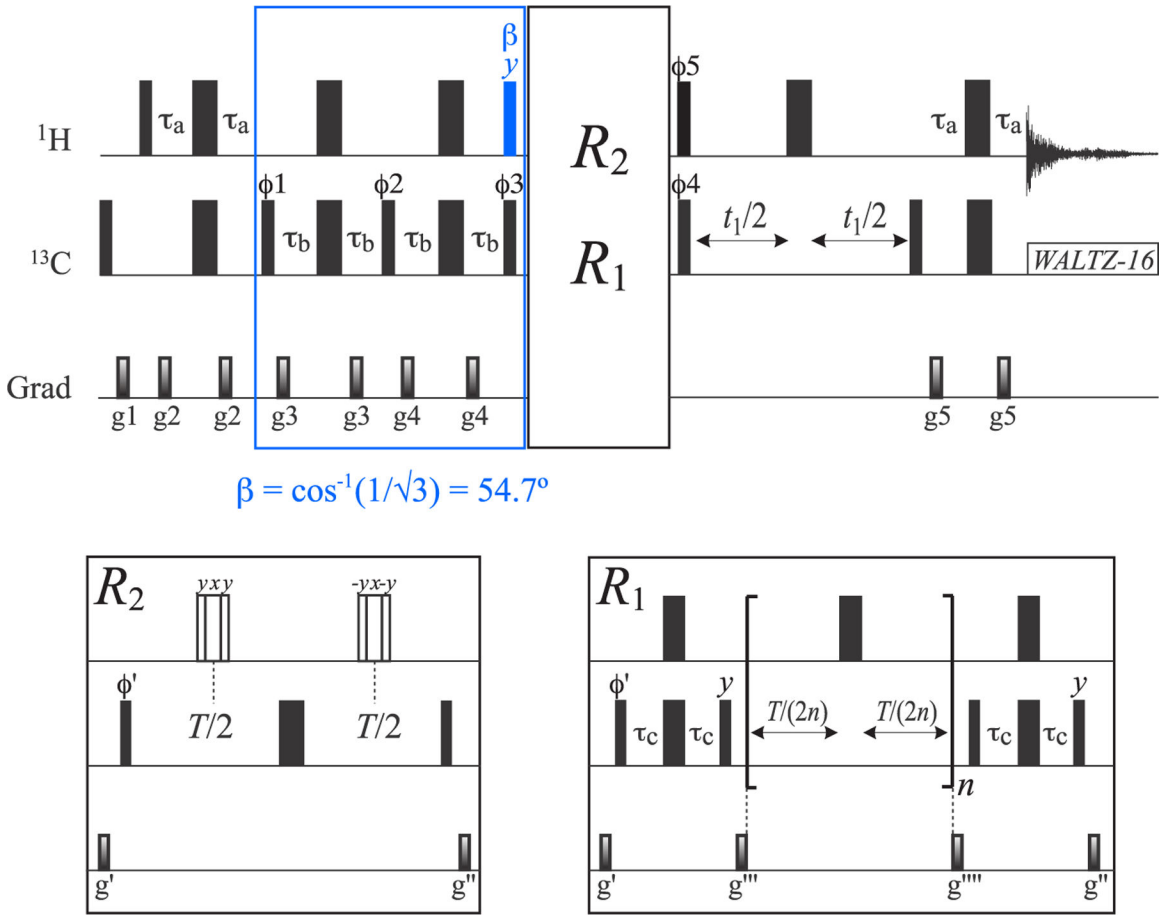

Figure 5.

Pulse scheme for the measurement of R_2 and R_1 relaxation rates of the outer ^{13}C magnetization modes of the $I = 3/2$ manifold ($L_1 \pm L_4$) in $^{13}CH_3$ methyl groups. All the parameters of the scheme (including delays) are the same as described in Figure 2. The ^1H pulse shown in blue is applied with the flip-angle $\beta = \cos^{-1}(1/\sqrt{3}) = 54.7°$. "Open" ^1H pulses in R_2 measurements are composite pulses of the 90°–240°–90° variety[29] that are applied with the phase-cycling indicated in the figure. Only the scheme for in-phase ($L_1 + L_4$) R_1 measurements is shown as used in practice. The durations and strengths of the pulsed-field gradients(ms; G/cm) are as follows: g1 = (1; 25), g2 = (0.4; 15), g3 = (0.3; 12), g4 = (0.35; 12), g5 = (0.4; 15), g′ = (1.2; 20), g″ = (0.8; 15), g‴ = (0.8; 20), and g⁗ = (0.6; 20). The phase cycle is as follows: $\phi 1 = 2(x), 2(-x)$; $\phi 2 = x, -x$; $\phi 3 = 4(x), 4(-x)$; $\phi 4 = x, -x$; $\phi 5 = 4(x), 4(-x)$; $\phi' = 4(x), 4(-x)$; and = receiver phase of $(x,-x,-x,x, -x,x,x,-x)$. Quadrature detection in t_1 is achieved via States-TPPI[28] incrementation of $\phi 4$.

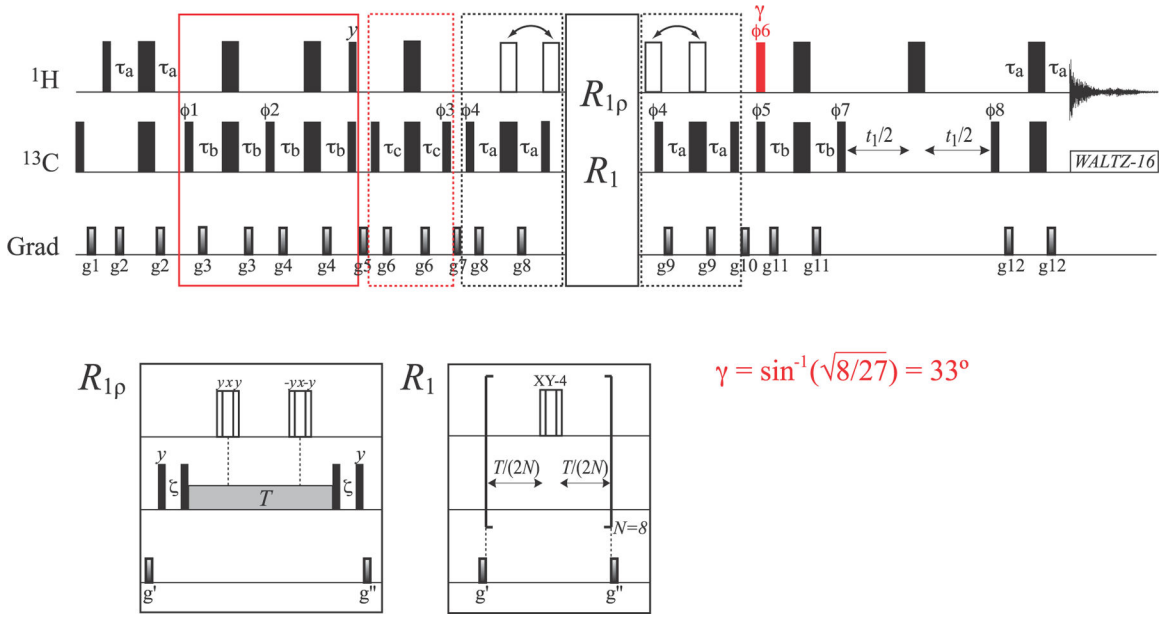

Figure 6.

Pulse scheme for the measurement of the $R_{1\rho}$ and R_1 relaxation rates of the inner ^{13}C magnetization mode of the $I = 3/2$ manifold ($L_2 \pm L_3$). All the parameters of the scheme (including delays) are the same as in Figure 2. The ^1H pulse shown in red is applied with flip angle $\gamma = \sin^{-1}(\sqrt{8}/27) = 33°$. "Open" ^1H 180° pulses of the main scheme (in the elements enclosed in dashed black boxes before and after the relaxation delays) are applied either simultaneously with ^{13}C 180° pulses (for in-phase measurements; $L_2 + L_3$) or outside the $2\tau_a$ elements (for antiphase measurements; $L_2 - L_3$) as indicated by arrows above the scheme. "Open" ^1H pulses in the R_2 and R_1 measurements are composites pulses of the 90°–240°–90° variety[29] that are applied using the phase-cycling indicated in the figure for the $R_{1\rho}$ measurements, and XY-4 phase-cycling[30,31] for R_1 measurements. Note that a total of eight ^1H π-pulses ($N = 8$) is used for R_1 measurements to avoid artifacts due to fast pulsing. The durations and strengths of pulsed-field gradients (ms; G/cm) are as follows: g1 = (1.0; 25), g2 = (0.4; 15), g3 = (0.3; 20), g4 = (0.35; 25), g5 = (1.4; 12), g6 = (0.2; 20), g7 = (0.8; 20), g8 = (0.5; 20), g9 = (0.4; 20), g10 = (1.0; 20), g11 = (0.3; 12), g12 = (0.5; 15), g′ = (0.8; 25), and g″ = (0.6; 20). The phase cycle is as follows: $\phi1 = 2(x), 2(-x)$; $\phi2 = x, -x$; $\phi3 = 2(x), 2(-x)$; $\phi4 = 2(x), 2(-x)$ for antiphase ($L_2 - L_3$) measurements and $2(y), 2(-y)$ for in-phase ($L_2 + L_3$) measurements; $\phi5 = x, -x$; $\phi6 = 4(x), 4(-x)$; $\phi7 = y, -y$; $\phi8 = x$; and receiver phase = $(x,-x,-x,x, -x,x,x,-x)$. Quadrature detection in t_1 is achieved via the States[32] incrementation of $\phi8$.

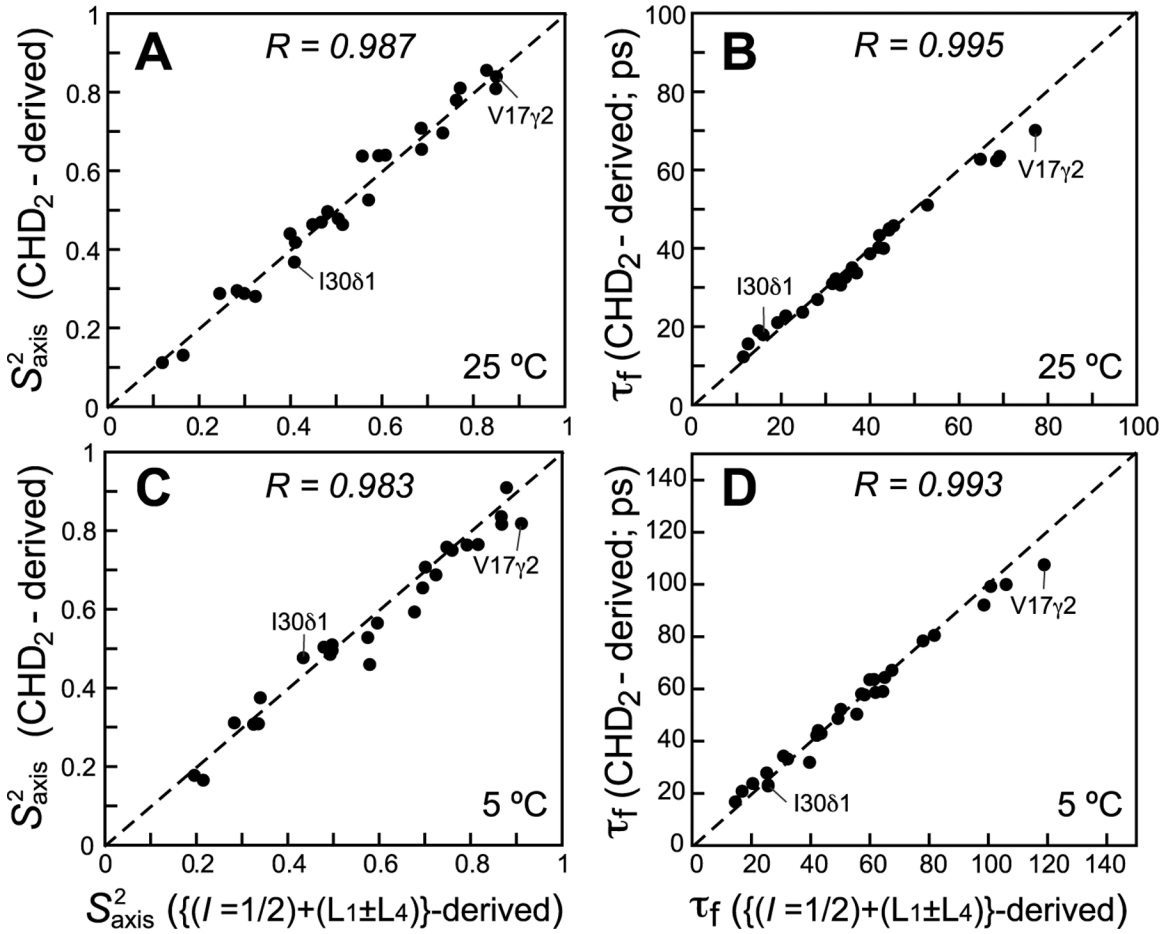

Figure 7.

Correlation plots comparing methyl-axis dynamics parameters derived from ^{13}C relaxation of the ($L_5 + L_6$) mode complemented with ^{13}C relaxation of ($L_1 \pm L_4$) in $^{13}CH_3$ methyls (x-axes) with those derived from the ^{13}C relaxation in $^{13}CHD_2$ methyls (y-axes) for an ILV-labeled sample of ubiquitin at 25 °C (upper row; (**A**) S^2_{axis} and (**B**) τ_f; 29 correlations) and 5 °C (lower row; (**C**) S^2_{axis} and (**D**) τ_f; 30 correlations). All data were collected at 600 MHz. Linear correlation coefficients are shown at the top of each plot. Dashed lines are drawn at $y = x$.